

Original Research

Distribution Characteristics of Groundwater Table in the Nagqu River Basin, Central Qinghai-Tibet Plateau

**Kebin Xia¹, Baisha Weng^{1,2*}, Xiaoyan Gong⁴, Shangbin Xiao³,
Wuxia Bi^{1,2}, Meng Li⁵, Denghua Yan¹**

¹State Key Laboratory of Simulation and Regulation of Water Cycle in River Basin, China Institute of Water Resources and Hydropower Research, Beijing 100038, China

²Yinshanbeilu National Field Research Station of Steppe Eco-hydrological System, China Institute of Water Resources and Hydropower Research, Hohhot 010020, China

³Engineering Research Center of Eco-Environment in TGR Region, Ministry of Education, College of Hydraulic & Environmental Engineering, China Three Gorges University, Yichang 443002, China

⁴China Fire and Rescue Institute, Beijing, 102202, China

⁵Department of Hydraulic Engineering, Tsinghua University, Beijing 100084, China

Received: 2 March 2023

Accepted: 26 June 2023

Abstract

Alpine regions' groundwater is crucial to the worldwide hydrological cycle. However, due to the harsh environmental conditions, the distribution and evolution characteristics await clarification. The study area was selected to be the Nagqu River Basin in the Nu-Salween River's source region. In 2019-2021, we gathered 88,000 monitoring data from nine observation wells and examined the spatiotemporal groundwater table changes in various permafrost zones and freeze-thaw cycles. During the freezing period, entirely frozen period, thawing period, and entirely thawed period, the groundwater table change rates in the permafrost zone were 2.14, 1.54, 1.55, and 2.01 times larger than in the seasonal frost zone, and fluctuation amplitudes were 1.97, 1.28, 1.01 and 1.31 times larger. The average groundwater table change rate and fluctuation amplitude were greatest during the entirely thawed period and lowest during the thawing period, with the maximum change rate reaching 3.64 cm/d during the entirely thawed period of 2019-2020 in the permafrost zone and the minimum change rate of 0.12 cm/d during the thawing period of 2019-2020 in the seasonal frost zone.

Keywords: groundwater table, freeze-thaw cycle, recharge and discharge, permafrost, alpine regions

Introduction

The Qinghai-Tibet Plateau (QTP), known as the “Asian Water Tower”, has a unique geographical environment, which sensitized the hydrological cycle to climate change [1-2]. Currently, the QTP is undergoing significant climate change, which has altered the atmospheric and hydrological cycles, thereby reconstructing the local environment [3]. Zhong et al. [4] found that the permafrost on the QTP is degrading with global warming, and the active layer thickness (ALT) is increasing [5-8]. Glacier melting and permafrost degradation lead to the continuous decline of water reserves in the QTP. The reduction in water reserves has changed the water cycle process in the basin, while permafrost degradation has changed the hydrogeology of the basin, further complicating groundwater dynamics in the alpine region [9-11]. The QTP contains complex types of groundwater, such as supra-permafrost groundwater, intra-permafrost groundwater, sub-permafrost groundwater, and deep groundwater. There are unique exchange methods between groundwater during different periods in alpine regions, which lead to different changes in groundwater table (GWT) from other regions [12-13]. Therefore, compared with surface water, people have less knowledge about the groundwater circulation system in alpine regions [14-15]. Analyzing how the plateau GWT changes are crucial to understanding the hydrological cycle evolution in the alpine basin.

Current research on groundwater in the alpine basin mainly focuses on changes in water temperature, quantity, and quality [16-18]. Limited by the few field experimental data, there is little research to reveal GWT changes () in alpine basins. Previous studies have shown that permafrost degradation leads to changes in hydrogeology and further complicates groundwater dynamics [19-20]. Models were used to simulate the impact of air and soil temperatures on GWT changes during different freeze-thaw periods, and temperatures are also one of the major influencing factors on GWT changes [21-23]. Hydrochemistry and isotope techniques are usually used to explore the exchange rate and the degree and rate of groundwater exchange with other water bodies, and can make a better judgment on the source, runoff, and discharge of groundwater. However, the changes of hydrochemistry and isotope are a long-term influence process, which cannot well explain the dynamic change characteristics of the current GWT [24-27]. At present, a large number of studies have been conducted on the factors influencing GWT changes in alpine regions, while these analyses cannot combine the influencing factors with the actual GWT changes because of the lack of measured GWT data, increasing the uncertainty of the analysis results. GWT changes suffer the combined effects of direct and indirect recharge, discharge, and lateral groundwater flow in the regional water cycle [28]. Influenced by the difference in recharge sources and freeze-thaw periods,

the groundwater in the alpine regions changes differently in different periods and hydrogeological conditions. The GWT changes can directly reflect the impact of recharge and discharge on groundwater, which is helpful for researchers to judge the main factors affecting GWT changes in different spatiotemporal conditions [29-30].

This study focuses on the Nagqu River Basin (NRB) in the Nu-Salween River's source area of QTP, which is a typical alpine region with variable hydrological cycle processes and wide distribution of permafrost and seasonal frost. Based on measured GWT data from 2019 to 2021 in the NRB, combining different permafrost types, freeze-thaw periods, and geological conditions, this paper analyzes the spatiotemporal change characteristics and causes under complex hydrogeological conditions of GWT in alpine basins. The results could provide a basis for groundwater development, utilization, and protection. The flow chart of the study is shown in Fig. 1.

Materials and Methods

Study Site

The NRB is situated in the middle of QTP (30°50'-32°44'N and 91°08'-93°01'E, Fig. 2a) where the Nu-Salween River originates. The basin has a surface area of 1.70×10^4 km² with an average altitude above 4,500 m (Fig. 2b) [2]. The NRB is located in a semi-arid climate zone, and the average annual precipitation is 482 mm (1950-2020) [31-32]. Precipitation fluctuates significantly throughout the year, with the greatest annual average precipitation of 113 mm in July and about 90% of precipitation concentrated from May to September [33]. The study site has a 180-day freezing period from October to April. The surface soil has a typical “graded structure” (fine sand and clay in the upper part, coarse sand, and gravel in the lower part). The main vegetation types are alpine grassland and meadow.

Hydrogeological Conditions

The north side of the study site is the Tanggula Mountains, and the Tanglha Mountains are located in the south. The northeastern basin is characterized by mountains and hills, with above 4800 m altitude, including a 3.53 km² glacier covered in snow all year. The outcrops are mostly bedrock, and the groundwater is mostly bedrock fracture water stored in bedrock fissures and fracture zones in different depths. The central part of the basin is dominated by plains and hills, with an average altitude of 4500 m. The outcrops are mainly quartz sandstone, mud shale, and siltstone. The groundwater is mainly stored in the pores (Fig. 2c). The southern and eastern parts of the basin are mainly plateau mountains, above 4800 m altitude, covered with seasonal freeze-thaw snow. The outcrops are mainly limestone, slate, and quartz sandstone. Because the

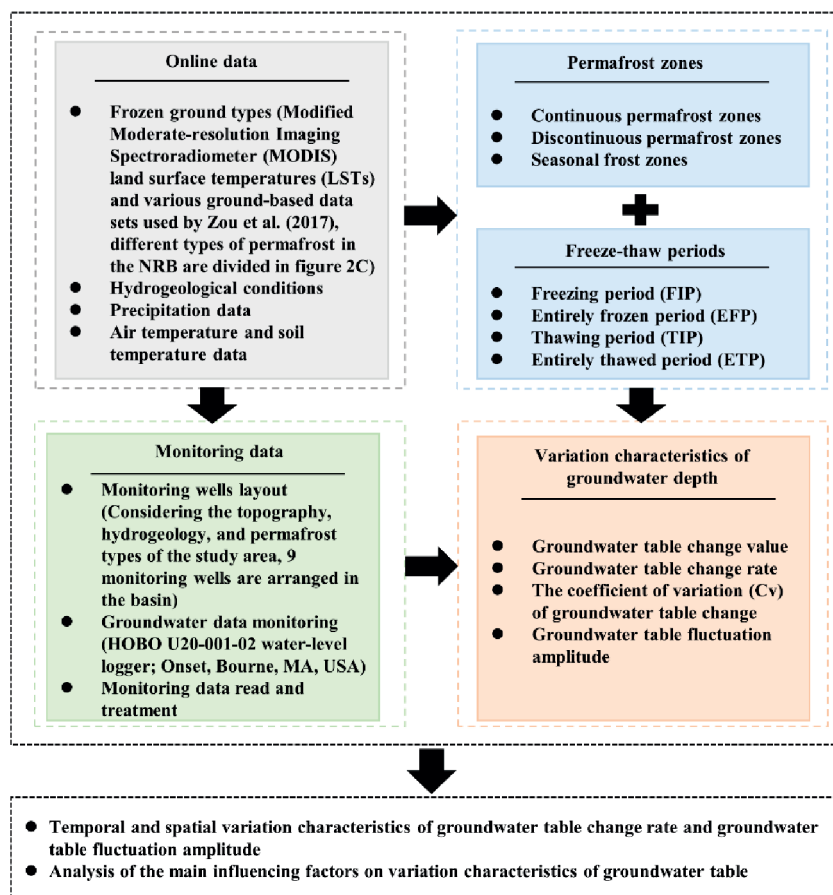


Fig. 1. Flow chart of the study.

groundwater is located at the crossroads of plain and mountain, the groundwater shows two characteristics of fissure water and pore water (Fig. 2c). Ice deposits are mainly distributed on the slopes of glaciers and mountains in the north, south, and east of the basin. The geological structure of the study area is complex and composed of East-West (EW) trending faults cut by North-West (NW), North-East (NE), and approximately North-South (NS) directional faults (Fig. 2c).

Permafrost type is directly related to altitude. The highest altitude in the northeast of the basin is 5875 m, which has both continuous and discontinuous permafrost (A1, B1 in Fig. 2c). The central part covered with seasonal frost occupies around 72% of the study area (C1 in Fig. 2c) [8]. In the east and south (>4800 m a.s.l.), there is both continuous and discontinuous permafrost, with discontinuous permafrost predominating (A2, B2, B3 in Fig. 2c). Several studies have reported that extreme climate events have exerted strong effects on permafrost environments [34-35], continuous permafrost is degrading to discontinuous permafrost, and discontinuous permafrost will degrade to seasonal frost [5, 36]. Permafrost degradation leads to changes in groundwater, and groundwater changes further contribute to permafrost degradation [37-38].

Groundwater Monitoring and Monitoring Wells Distribution

Considering the topography, hydrogeological conditions, and actual situation of the study site, the GWT at nine wells in the basin was monitored for a long time in September 2019. The GWT in each well was monitored by pressure transducers (HOB0 U20-001-02 water-level logger; Onset, Bourne, MA, USA). The measurement accuracy of GWT is ± 0.05 cm, the temperature measurement range is -20°C to 50°C , and the data recording interval is 2h. A local habitant is arranged to guarantee the working status of the installed instruments to ensure data reliability.

Monitoring well WW2 is located in zone B2, and monitoring wells WW1 and WW3 are located in zone B3, which are discontinuous permafrost zones. Monitoring well WW1 is located in zone A1, which is the continuous permafrost zone (Table 1). Monitoring wells WW5-WW9 are located in zone C1, which is the seasonal frost zone (Table 2).

Data Acquisition and Period Division

By September 2021, the pressure transducers had recorded approximately 88,000 GWT data. Eliminate

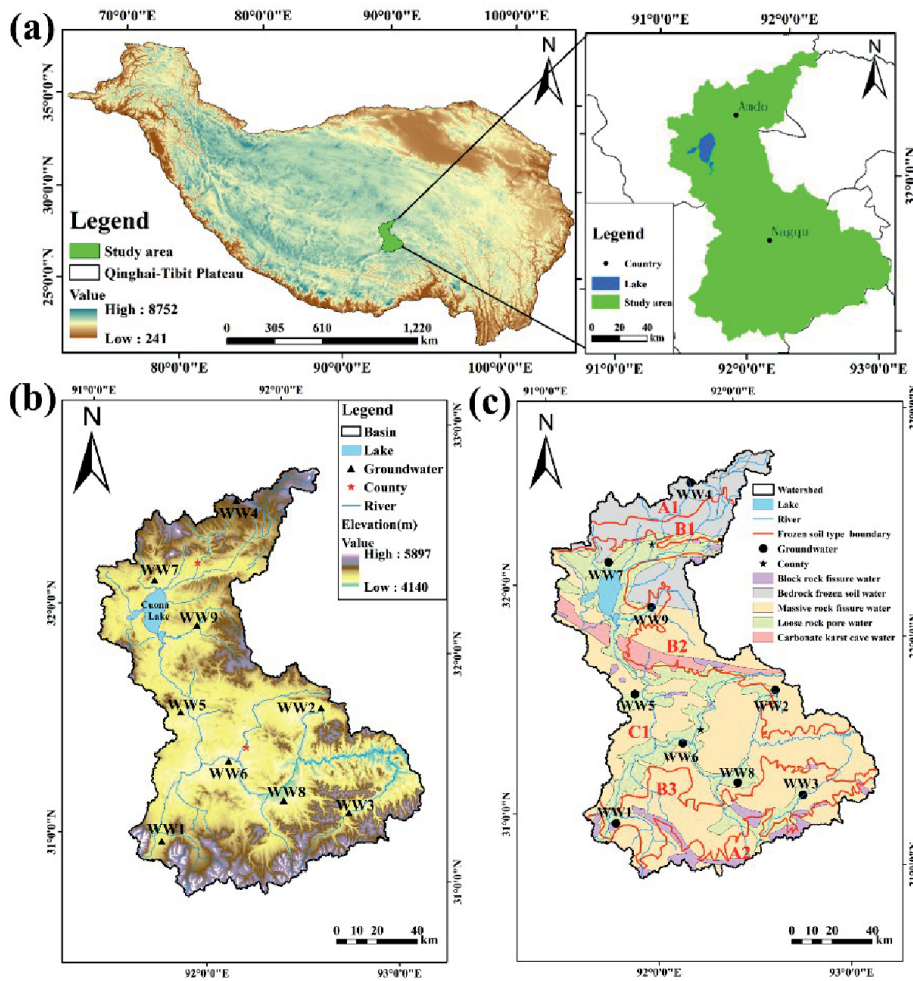


Fig. 2. The study area's location is shown in a), and the sites of the groundwater table monitoring wells are shown in b) hydrogeological and permafrost types in c). The continuous permafrost zone is denoted by (A1-A2), the discontinuous permafrost zone by (B1-B3), and the seasonal frost zone by (C1).

large abrupt changes and human interference during data recording, ensuring the integrity and accuracy of data when calculating the daily average GWT. To improve the reliability of the data, the nine monitoring wells in this study were divided into three categories based on permafrost types to adjust for the short period of the monitoring sequence.

The air temperature and precipitation data were downloaded from <http://www.meteomanz.com/>, and the soil temperature was downloaded from https://appears.earthdatacloud.nasa.gov/MODIS_Land_Surface_Temperature.

By counting the number and frequency of short-duration freeze-thaws in the NRB and calculating the

Table 1. Spatial information of monitoring wells in permafrost zones.

Monitoring well	WW1	WW2	WW3	WW4
Latitude	31°1'24"	31°41'44"	31°15'58"	32°33'10"
Longitude	91°40'39"	92°25'22"	92°38'19"	91°50'3"

Table 2. Spatial information of monitoring wells in seasonal frost zones.

Monitoring well	WW5	WW6	WW7	WW8	WW9
Latitude	31°35'54"	31°24'34"	33°9'53"	31°16'16"	31°59'21"
Longitude	91°41'11"	91°58'24"	91°27'19"	92°17'22"	91°42'37"

short-duration freeze-thaw intensity by combining freezing temperature difference, freezing time difference, freezing calendar time, freeze-thaw temperature difference, freeze-thaw time difference, and freeze-thaw calendar time, Zhou et al. [39] found that the high-intensity and high-frequency freeze-thaw events were mainly concentrated in the months of October-December and March-May, and the freeze-thaw characteristics were jointly influenced by temperature, altitude, slope, soil physical properties, and soil depth. To analyze the effect of the freeze-thaw cycles on the GWT dynamics, combining the short duration freeze-thaw months and the changes in GWT [2, 40], this study divided the freeze-thaw periods into four stages: a freezing period (FIP, September 1 to November 30), an entirely frozen period (EFP, December 1 to March 15 of the following year), a thawing period (TIP, March 16 to May 31), and an entirely thawed period (ETP, June 1 to August 31).

Results

Variation Characteristics of Precipitation, Soil Temperature, Air Temperature, and Average Groundwater Table in the NRB

According to the GWT data (average GWT of 9 monitoring wells), precipitation, air temperature, and soil temperature in the NRB from 2019 to 2021 (Fig. 3), the curves showed a “falling-rising” V-shaped

change. Air temperature and soil temperature almost simultaneously decreased from August to next January and increased from February to July, but the fluctuation of air temperature was greater than soil temperature. The GWT ascended from mid-March to August and descended from September to next mid-March. The soil temperature had risen to 0 °C when the GWT began to rise in mid-March. There is a time delay between soil temperature and GWT increase. Soil thawing may be an important condition for the groundwater to start receiving the recharge. The time soil temperature decreasing below 0°C in 2020-2021 (November 4) was later than in 2019-2020 (October 27), and raising to 0°C was earlier (Fig. 3). The variable range of soil and air temperature in 2020-2021 was smaller than in 2019-2020, and the variable range of GWT was also smaller in 2019-2020. The variable range of soil temperature may directly affect the variable range of GWT. Precipitation began to increase in April, and the GWT gradually ascends. The GWT ascends slowly during the TIP, with an average ascending value of 0.39 m from mid-March to the end of May (average ascending value of two years). The precipitation increases dramatically during the ETP, which is account for 77.9% of the annual precipitation. The air and soil temperatures reach the maximum values during the ETP, and the ascending value of GWT was 1.26 m when precipitation and infiltration have the highest influence on groundwater. Soil temperature and GWT began to descend on August 20 and August 17, respectively. Different from the ascending period, the descending GWT has a rapid response to the freezing

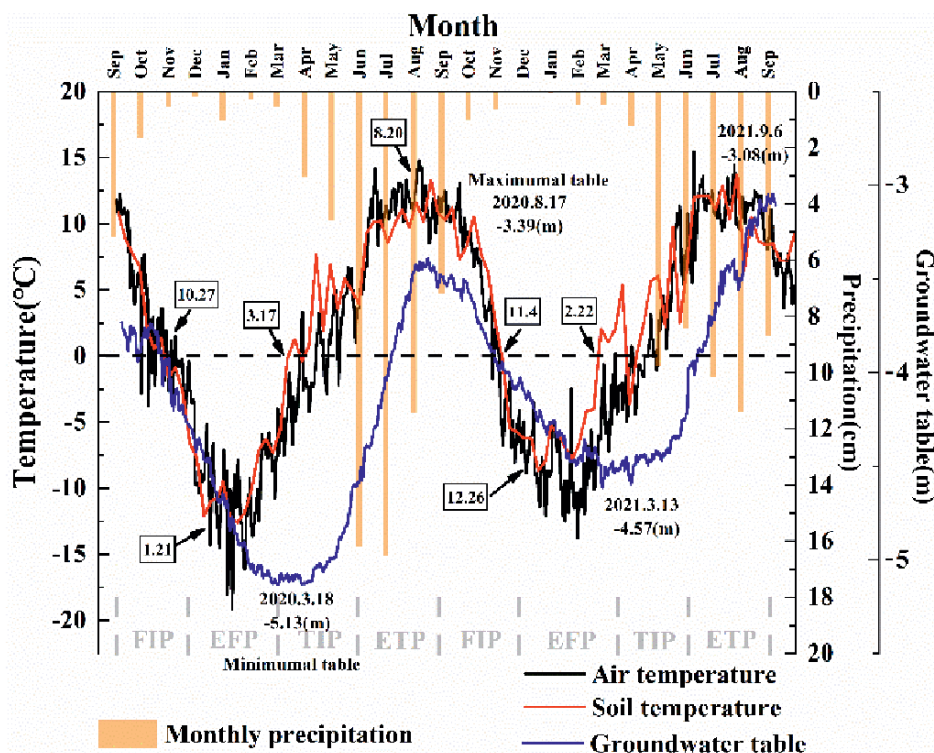


Fig. 3. Curves of precipitation, air temperature, soil temperature, and average groundwater table from 2019 to 2021.

process. The average descending value of GWT during FIP was 0.75 m, which had little difference from that during EFP (0.71 m).

Spatiotemporal Change Characteristics of Groundwater Table

September to mid-March is the declining period of GWT, and mid-March to September is the rising period of GWT. The groundwater tables in monitoring wells WW4 and WW1 were shallow, and groundwater in WW4 belongs to bedrock fracture water, and the water table fluctuates significantly, but because there are glaciers and snow covered nearby, the recharge source is diverse and recharges the groundwater. WW1 groundwater belongs to loose rock pore water, which is strongly influenced by precipitation and surface water, and the GWT was shallow. The maximum GWTs are -2.49 m and -1.69 m, and the minimum GWTs are -3.36 m and -2.65 m, with a difference of 0.87 m and 0.96 m, respectively. Monitoring wells WW2 and WW3 were deeper, both belong to bedrock fracture water, and the groundwater is at the junction of plains and mountains, with large topographic relief and lack of recharge sources, with obvious seasonal changes, the maximum GWTs are -5.51 m, -3.82 m, and the minimum GWTs are -8.08 m, -7.71 m, with a difference of 2.57 m and 3.89 m, respectively. WW7 and WW9 sites are located in the middle and upper reaches of the basin, groundwater belongs to the loose rock pore water and massive rock fissure water, adjacent to the lake. WW6, WW5, WW8 sites are located in the middle and lower reaches of the basin, groundwater belongs to loose rock pore water, pore water interacts with precipitation and surface water frequently. 1.87 m, 0.89 m, 1.24 m, 0.99 m, 0.54 m difference between the maximum and minimum GWT of WW5, WW6, WW7, WW8, WW9 monitoring wells respectively.

To further reflect the spatiotemporal change characteristics of GWT, we introduce the coefficient of variation (Cv), which can reflect the dispersion degree of variables (Table 3). $Cv < 10\%$ belongs to weak variation, $10\% < Cv < 100\%$ belongs to moderate variation, and $Cv > 100\%$ belongs to strong variation. According to Table 3, the Cv of GWT in the permafrost zone varies from 2.57% to 15.92% over four periods, with both weak and moderate variation, while the Cv of GWT in the seasonal frost zone varies from 0.51% to 9.54% over the four periods, with a weak variation. This demonstrates that the GWT varies more noticeably in the permafrost zone than in the seasonal frost zone. The GWT has spatial variability. The average Cvs of GWT in the seasonal frost zone are 4.59% in the FIP, 6.66% in the EFP, 4.14% in the TIP, and 3.12% in the ETP. Moderate variation occurs in the FIP and ETP of the permafrost zone. The FIP and ETP had higher Cv than the EFP and TIP. The GWT has temporal variability.

Table 4 shows the GWT change value and change rate in four periods. In addition to the spatiotemporal

Table 3. The statistical characteristic value of groundwater table in different periods in Nagqu River Basin.

Monitoring wells	Periods	Average table (m)	Standard deviation	CV value (%)
WW1	FIP	-2.77	0.119	4.30
	EFP	-3.19	0.145	4.55
	TIP	-3.26	0.112	3.44
	ETP	-2.73	0.198	7.25
WW2	FIP	-6.25	0.438	7.00
	EFP	-7.71	0.227	2.94
	TIP	-7.95	0.204	2.57
	ETP	-6.41	0.948	14.79
WW3	FIP	-5.66	0.390	6.89
	EFP	-7.00	0.444	6.34
	TIP	-7.53	0.247	3.28
	ETP	-5.07	0.807	15.92
WW4	FIP	-1.86	0.296	15.91
	EFP	-2.55	0.173	6.78
	TIP	-2.54	0.146	5.75
	ETP	-1.84	0.239	12.99
WW5	FIP	-3.61	0.107	2.96
	EFP	-4.37	0.277	6.34
	TIP	-4.48	0.219	4.89
	ETP	-3.25	0.304	9.35
WW6	FIP	-3.50	0.280	8.00
	EFP	-4.29	0.130	3.03
	TIP	-4.43	0.109	2.46
	ETP	-3.87	0.168	4.34
WW7	FIP	-2.65	0.122	4.60
	EFP	-2.87	0.152	5.30
	TIP	-3.03	0.058	1.91
	ETP	-2.63	0.251	9.54
WW8	FIP	-1.99	0.135	6.78
	EFP	-2.36	0.089	3.77
	TIP	-2.30	0.134	5.83
	ETP	-1.70	0.137	8.06
WW9	FIP	-6.14	0.036	0.59
	EFP	-6.48	0.147	2.27
	TIP	-6.82	0.035	0.51
	ETP	-6.49	0.131	2.02

Table 4. The change value and rate of groundwater table in different periods in Nagqu River Basin.

Monitoring wells	Year	FIP		EFP		TIP		ETP	
		Change value (cm)	Rate (cm/d)	Change value (cm)	Rate (cm/d)	Change value (cm)	Rate (cm/d)	Change value (cm)	Rate (cm/d)
WW1	19-20	66.5	0.81	74.4	0.70	63.4	0.82	116.8	1.27
	20-21	91.0	0.40	105.0	0.24	77.0	0.25	102.0	0.24
WW2	19-20	151.4	1.85	85.9	0.81	98.6	1.28	335.1	3.64
	20-21	175.6	1.93	108.6	1.03	65.5	0.85	320.5	3.14
WW3	19-20	117.0	1.43	150.4	1.42	96.7	1.26	241.0	2.62
	20-21	132.0	1.45	126.5	1.21	63.2	0.82	420	2.65
WW4	19-20	92.3	1.13	114	1.08	69.1	0.90	103.3	1.12
	20-21	115.8	1.27	34.9	0.33	55.0	0.71	76.8	0.75
WW5	19-20	26.6	0.32	129.8	1.23	83.7	1.09	150.9	1.64
	20-21	71.1	0.78	53.3	0.51	83.2	1.08	69.2	0.68
WW6	19-20	122.6	1.50	57.2	0.54	64.9	0.84	116.5	1.27
	20-21	70.5	0.78	40.1	0.38	15.5	0.20	22.1	0.22
WW7	19-20	18.6	0.23	82.4	0.78	29.1	0.38	167.9	1.83
	20-21	66.0	0.73	31.5	0.30	22.5	0.29	111.9	1.10
WW8	19-20	54.9	0.67	25.4	0.24	46.1	0.60	74.3	0.80
	20-21	53.7	0.59	44.1	0.42	49.7	0.65	62.2	0.61
WW9	19-20	24.0	0.29	20.7	0.20	9.3	0.121	27.7	0.30
	20-21	11.0	0.12	99.7	0.95	24.3	0.32	119.3	1.17

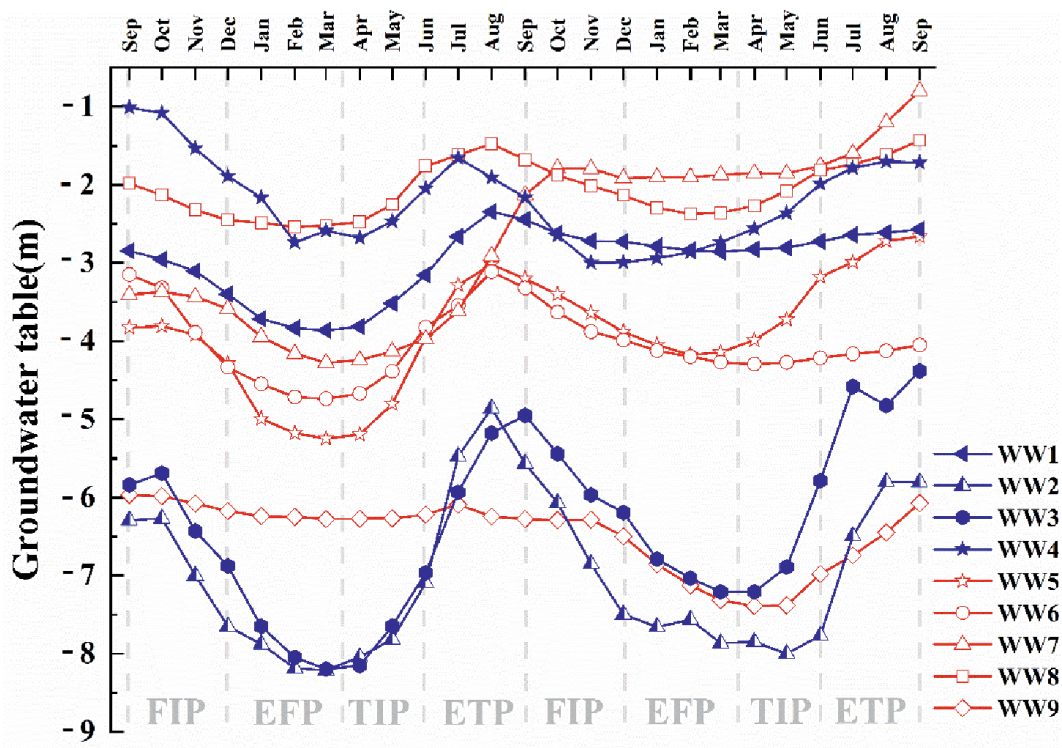


Fig. 4. The groundwater table monitoring wells (WW1-WW9) from 2019 to 2021. WW1-WW4 are in the permafrost zone (WW1 in the continuous permafrost zone), and WW5-WW9 are in the seasonal frost zone.

changes in the dispersion of the GWT, there are also spatiotemporal changes in the GWT change value and change rate. In the permafrost zone, the GWT change values were all less than 100 cm during the TIP and generally greater than 100 cm during the FIP, EFP, and ETP, with a greater average GWT change rate during the ETP. The seasonal frost zone in the ETP experiences the biggest change in GWT, with some change values surpassing 100 cm. The GWT change values throughout the remaining periods, on the other hand, are frequently less than 100 cm.

Temporal Variations of Groundwater Table Fluctuation Amplitude in the NRB

In seasonal frost zones, the IQR first drops (3.4 cm to 2.7 cm), then increases (2.7 cm to 3.05 cm) (March-May) (Fig. 5a). The Q_3 continues to decrease, suggesting that the increasing fluctuation amplitude of GWT decreases. The lower discharge capacity continues to decline. The Q_1 falls by 0.1 cm in April and increases by 0.8 cm in May. The decreasing fluctuation amplitude of GWT has no obvious change in April, rising in May, showing that the lower recharge capacity increases in May. The Maximum (MAX) falls in April (4.90 cm to 3.20 cm) and then rises in May (3.20 cm to 4.10 cm), suggesting that the higher discharge capacity decreases in April and increases in May. The reduced discharge capacity may be due to meltwater recharge to surface water, reducing groundwater recharge to surface water. As the soil thaws, when groundwater delivery channels increase, evaporation and groundwater discharge capacity are enhanced. The Minimum (MIN), which has been rising steadily and growing dramatically in May, shows that the higher groundwater recharge capacity significantly improve in May.

The ETP is from June to August. When precipitation reaches its maximum, air and soil temperatures rise to their highest (Fig. 3), and the IQR increases significantly in June and July and decreases in August (Fig. 5a). The Q_3 keeps growing, showing that the lower discharge

capacity gradually rises throughout the ETP. Q_1 reaches its peak in June before declining, indicating that the lower recharge capacity reaches its peak in June before declining. The MAX and MIN are higher in June and July and lower in August. The higher recharge and discharge capability are higher in June and July, falling in August. There are many outliers below the boxplot during the ETP, and groundwater occasionally experiences the highest recharge effects, which may be connected to heavy precipitation. The boxplot are all negatively skewed during the ETP, recharging has a bigger effect on groundwater, and the GWT reaches the maximum.

During the FIP, the IQR does not vary considerably in September, but it significantly decreases in October before slightly increasing in November (Fig. 5a). From September to October, the Q_3 , Q_1 , MAX, and MIN decrease significantly, and the fluctuation amplitude of the ascending and descending GWT decreased significantly, indicating the recharge and discharge capacity of groundwater declined considerably. The GWT fluctuation amplitude reaches a very low value in October. The fluctuation amplitude of GWT increases from October to November, indicating an increase in groundwater recharge and discharge capacity. The outliers above the boxplot dramatically increase in November, and the boxplots are all negatively skewed, suggesting that the groundwater's changes are dominated by the discharge capacity as the table gradually descends.

December to next February is the EFP, with the IQR increasing significantly in December, decreasing in January, and increasing slightly in February (Fig. 5a). The Q_3 and MAX increase significantly in December, and the MAX reaches the maximum in December, indicating that the discharge capacity of groundwater in the seasonal frost zone reaches its highest in December, which may be related to groundwater recharge to surface water. The recharge and discharge capacity slightly decline in January as the temperature reaches its lowest point (Fig. 3), while it slightly increases in February.

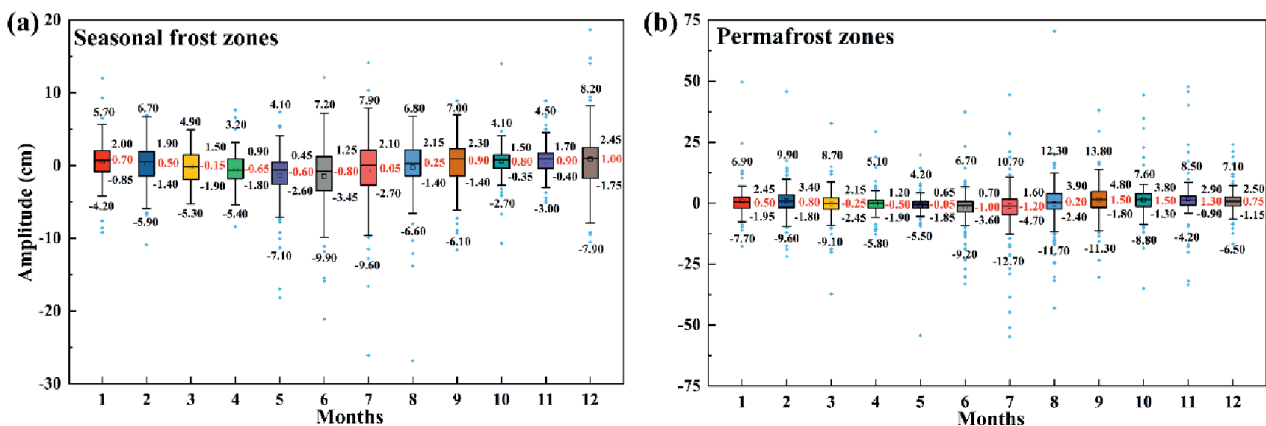


Fig. 5. Temporal fluctuation amplitude of groundwater table in seasonal frost zones a) and permafrost zones b).

The GWT reaches its lowest point during the EFP when the discharge dominates the change in groundwater.

From March to May, the IQR, Q_1 , Q_2 , MAX, and MIN gradually decrease, and the effects of recharge and discharge gradually decrease (Fig. 5b). The boxplots are positive skewness, the groundwater is more strongly influenced by recharge, and the GWT gradually ascends. During the TIP, the maximum GWT fluctuation amplitude in the permafrost zone occurs in May, one month later than in the seasonal frost zone.

Both Q_3 and MAX grow from June to August, and the discharge capacity continues to rise (Fig. 5b). The impact of recharge on groundwater grows dramatically in June and July, peaks in July, and then begins to decline in August. The discharge capacity in the seasonal frost zone began to decrease in August, while the groundwater discharge capacity in the permafrost zone continue to rise in August and September.

During the FIP from September to November, the minimum QIR occurs in November, which is one month later than the seasonal frost zone (Fig. 5). The Q_3 continues to decrease, the influence of the lower discharge effect on groundwater reduces, and the influence of the higher discharge effect first decreases and then increases. The impact of recharge on groundwater continues to decrease. Groundwater is mostly discharged at this time, and the table gradually descends.

From December to next February, the groundwater discharge capacity of the permafrost zone decreases in December (Fig. 5b), while the seasonal frost zone groundwater discharge capacity is the highest during the year in December (Fig. 5a). There is no significant change in discharge capacity in January and a slight increase in February. The recharge on groundwater is also slightly elevated in December and January, with no significant change in February, when discharge has a greater impact on groundwater and GWT descends to the minimum.

Spatial Variations of Groundwater Table Fluctuation Amplitude in the NRB

Comparison of Groundwater Fluctuation Amplitude in Permafrost and Seasonal Frost Zones

The fluctuation amplitude of GWT in the permafrost zone in the FIP, EFP, and ETP is greater than in the seasonal frost zone, with a maximum difference of two times in the FIP and a small difference in the TIP. The ranges of MAX-MIN are the largest in the ETP, 16.6 cm, and 21.7 cm, respectively, implying that groundwater is most obviously recharged and discharged during the ETP. For the outliers, the maximum upper and lower outliers are 1 m and 0.5 m respectively. The groundwater recharge and discharge capacity in the permafrost zone reaches the maximum in the ETP during the year, but the MAX does not differ much from the freezing period, implying that the groundwater in the permafrost zone usually does not reach the maximum discharge capacity during the ETP (Fig. 6b). The fluctuation amplitude of the GWT in the EFP is still more significant, and the range of upper outliers is larger, which indicates that groundwater still has a high discharge capacity in the EFP. The maximum difference for the fluctuation amplitude of groundwater during the different periods of the year in the permafrost zone is 2 times (Fig. 6b), while the maximum difference in the seasonal frost zone is 1.6 times (Fig. 6a), and the groundwater in the permafrost zone has greater intra-annual variation.

Comparison of Groundwater Fluctuation Amplitude in Continuous Permafrost and Discontinuous Permafrost Zones

The permafrost zone is split into continuous and discontinuous permafrost to assess the effects of permafrost degradation on GWT. It can be seen that

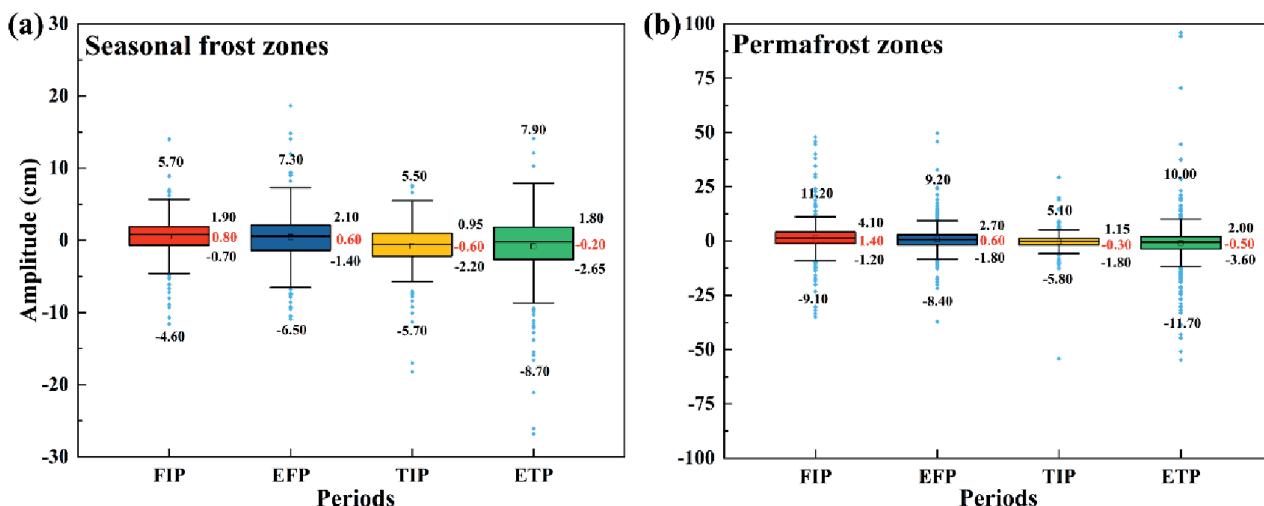


Fig. 6. Fluctuation amplitude of groundwater table in seasonal frost zones a) and permafrost zones b).

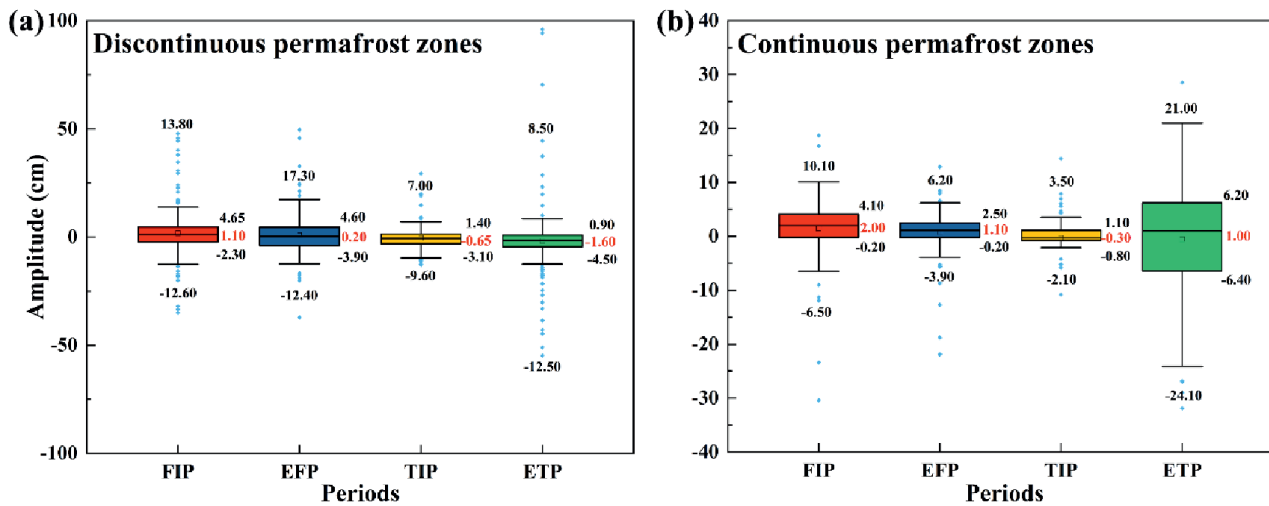


Fig. 7. Fluctuation amplitude of groundwater table in discontinuous permafrost zones a) and continuous permafrost zones b).

during the ETP, the fluctuation amplitude of GWT in the continuous permafrost zone is 2.15 times greater than in the discontinuous permafrost zone. The GWT fluctuation amplitude in the discontinuous permafrost zone is higher during the rest of the periods, which is about three times greater than the continuous permafrost zone during the EFP (Fig. 7). Particularly in the continuous permafrost zone, where the range of MAX-MIN exceeds 45.1 cm, the range of outliers during the ETP is the biggest, and groundwater is susceptible to the strongest recharge and discharge (Fig. 7a). The MAX of the FIP and the EFP can be seen that the discharge capacity of groundwater during the freezing periods is still larger in the discontinuous permafrost zone (Fig. 7a), while the fluctuation of groundwater in the freezing periods is significantly reduced in the continuous permafrost zone (Fig. 7b). Groundwater in the continuous permafrost zone has a greater intra-annual variation with a maximum difference of 8 times, compared to a maximum difference of 1.59 times in the discontinuous permafrost zone.

Discussion

The Groundwater Table Change Rate and Fluctuation Amplitude in the Permafrost Zone are Greater than the Seasonal Frost Zone with more Significant Recharge Capacity During the Entirely Thawed Period and more Significant Discharge Capacity During the Entirely Frozen Period

When compared to the seasonal frost zone, the permafrost zone's GWT average change rates are 2.14, 1.54, 1.55, and 2.01 times greater during the FIP, EFP, TIP, and ETP. In the NRB, the variation in GWT is seasonal, and the GWT, air temperature, soil temperature, and precipitation all exhibit a "falling-rising" V-shape change (Fig. 3). This "falling-rising"

feature was also noted in earlier studies of alpine basins [38, 41], and we discovered that this feature is highly variable in spatiotemporal. Unlike the rapid response of freezing to soil temperature change, the response of thawing to soil temperature change is a slow process [42], and there is a time delay between the process of soil temperature and GWT increase [12]. Therefore, the GWT does not ascend when the soil temperature increase from February to March. The minimum value of the GWT occurs in mid-March and the maximum value occurs in September (Fig. 3).

The GWT fluctuation amplitudes in the permafrost zone are frequently 1.97, 1.28, and 1.31 times larger in the FIP, EFP, and ETP, compared to the seasonal frost zone (Fig. 6). The fluctuation amplitude in the TIP is not statistically different. Comparing the GWT fluctuation amplitude over four different periods in permafrost zones revealed that the maximum variation in permafrost zones over four periods is 2 times (Fig. 6b), with a greater intra-annual change, whereas the maximum variation in seasonal frost zones over four periods is 1.6 times (Fig. 6a), with a weaker intra-annual change. GWT fluctuation amplitude suffers the combined effects of direct and indirect recharge, discharge, and lateral groundwater flow in the regional water cycle [28]. The fluctuation amplitude of GWT in the permafrost zone has not only bigger intra-annual variation but also greater spatial variability. The effects of recharge and discharge on groundwater in the permafrost zone are stronger. Previous studies had also revealed supra-permafrost groundwater with low mineralization, short residence times, a variety of groundwater recharge sources, and quick discharge paths in permafrost zones [43-44].

The GWT fluctuation amplitude during the ETP has the highest value, and the MIN-MAX ranges are 16.6 cm and 21.7 cm, respectively (Fig. 6), showing that the capacity for recharge and discharge peaks during

the ETP [13]. Additionally, the lower outliers during the ETP are the largest within the year, and the recharge capacity is the most significant during the ETP (Fig. 6). The GWT fluctuation amplitude in the permafrost zone reaches 1 m during the ETP (upper outliers), but the range of MAX is not much different from the freezing period and the groundwater usually does not reach its maximum discharge capacity [45] (Fig. 6b). Because the fluctuation amplitude of GWT in the discontinuous permafrost zone and the seasonal frost zone is bigger during the EFP (Fig. 6a and 7a), groundwater still has a high discharge capacity during the freezing period. In the freezing period, particularly in the EFP, the fluctuation amplitude of GWT in the continuous permafrost zone is seriously reduced (Fig. 7b). Previous studies had found that groundwater flow in permafrost zones is very limited during the freezing period, limiting groundwater recharge and discharge capacity [13, 15], but we found that this phenomenon occurs mainly in continuous permafrost zones, and groundwater discharge capacity in discontinuous permafrost zones remains significant during the freezing period.

Hydrogeological Conditions, Types of Water Supply, and Discharge Methods are the Main Factors of the Groundwater Table Change

One of the factors influencing the change in GWT is the hydrogeological conditions. Groundwater in the permafrost zone of the NRB is primarily bedrock fissure water, showing inhomogeneity and anisotropy, but the

groundwater in the seasonal frost zone is primarily pore water, and the hydraulic connection is stronger. The groundwater flow capacity is different as a result of the variation in hydrogeological conditions, affecting the GWT changes [19, 46].

The types of water supply are another factor affecting the GWT change. Groundwater in the permafrost zone is recharged by a combination of meltwater, surface water, and precipitation [47-48]. Gong et al. [45] analyzed the groundwater and meltwater collected in the NRB by isotopic and hydrochemical analysis, which proved that the groundwater in the permafrost zone of the NRB is recharged by glacial and snow meltwater. The reserves of ground ice in permafrost zones are more abundant than groundwater, and the melting of ground ice also recharges groundwater [49]. Seasonal frost zones are mostly plains and river valleys, which are groundwater flow and catchment areas. These areas are laterally recharged by groundwater from permafrost zones, while surface water and precipitation also recharge groundwater in seasonal frost zones [12]. Influenced by the monsoon climate [50], nearly 90 % of precipitation during the year occurs during the ETP [2], and when the ALT melts to its maximum depth, precipitation also reaches its maximum, and infiltration recharge to groundwater reaches its maximum. The recharge of runoff from glacial, snow, and glacial sediment meltwater reaches its maximum during the ETP [51-53], and meltwater not only directly recharges groundwater but also indirectly increases the recharge of groundwater from surface water.

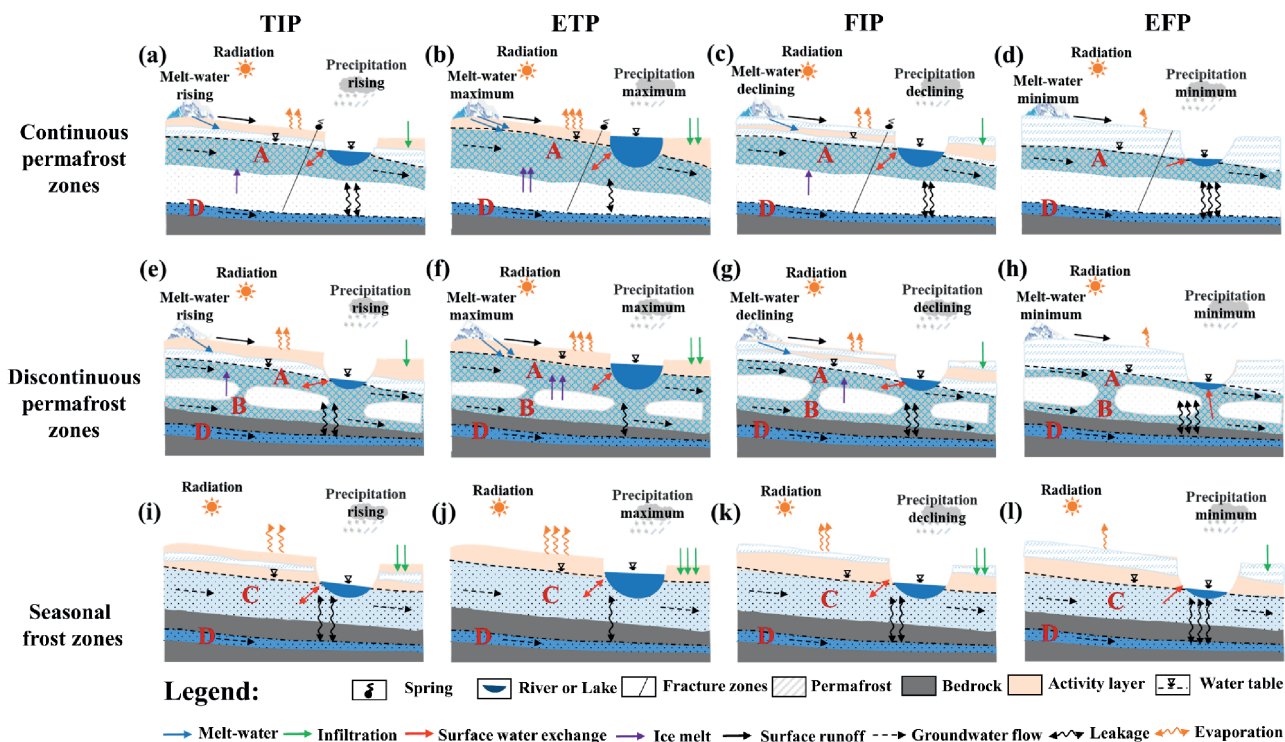


Fig. 8. Conceptual model of groundwater recharge and discharge characteristics. The aquifers in (A), (B), (C), and (D) are the supra-permafrost, sub-permafrost, shallow, and deep aquifer, respectively.

The differences in discharge modes are also the main factor affecting the change in GWT. Due to the uneven contact between bedrock in the permafrost zone, groundwater discharge from bedrock fractures as springs [45]. Because of the higher altitude in the permafrost zone, groundwater recharges laterally downstream and also recharges surface water during the freezing periods [54]. The main modes of groundwater discharge in seasonal frost zones are the recharge of surface water and evaporation [45]. In discontinuous permafrost and seasonal frost zones, the discharge effect is more pronounced during the EFP and ETP (Fig. 6a and 7a). Previous studies have found that during the freezing periods, when glaciers and snow are frozen to the maximum extent, there are still base flows in rivers, and these base flows are mostly from groundwater recharge [55-56]. Guo et al. [57] discovered that during the freezing periods, groundwater becomes the primary source of recharge to surface water through changes in major ions, ^{18}O , and ^2H , and the contribution of groundwater to rivers even exceeds 95% [13]. Recharge to surface water also becomes the primary mode of groundwater discharge during this time. During the ETP, evaporation accelerates dramatically and takes over as the primary groundwater discharge method. The conceptual model of groundwater recharge and discharge characteristics is shown in Fig. 8.

Uncertainty Analysis

The groundwater change pattern under various permafrost types and periods is evident in our data, which enriches our understanding of groundwater changes in alpine regions and supports earlier groundwater research findings in the NRB and other alpine basins. The influencing factors of GWT change are in qualitative analysis, which cannot explain the specific GWT change phenomenon because of the complexity of the hydrogeology for the alpine basin and the lack of a meteorological-soil-groundwater monitoring system with high monitoring frequency. Previous studies had shown that deep groundwater recharges shallow groundwater during the freezing period and permafrost degradation accelerates this exchange [13, 19, 21], and our results also show that the recharge effect of seasonal frost zone and discontinuous permafrost zone is enhanced during the freezing period, but the exchange mode and the intensity of the exchange are uncertain. In the future, we hope to quantitatively analyze the groundwater changes in the NRB by continuing monitoring and combining them with the model.

Conclusion

This study describes the GWT change rate and fluctuation amplitude under different permafrost types

and different periods in the NRB and analyzes the main influencing factors leading to the changes. The main findings are as follows:

The GWT change rate in the permafrost zone ranges from 0.24 cm/d to 3.64 cm/d, while the change rate in the seasonal frost zone ranges from 0.12 cm/d to 1.83 cm/d. The average change rate in the permafrost zone is greater than that in the seasonal frost zone in four periods. The maximum GWT change rate occurs during the ETP and the minimum rate occurs during the TIP. The GWT change rate in the NRB exhibits spatiotemporal variability.

Due to the stronger recharge and discharge of permafrost zones, the fluctuation amplitude of GWT in permafrost zones is greater than that in seasonal frost zones. The seasonal frost zone fluctuates by a maximum of 1.6 times in the four periods with a weaker intra-annual change, compared to the permafrost zone, which fluctuates by a maximum of 2 times with a greater intra-annual change. There are spatiotemporal variations in the GWT fluctuation amplitude.

The fluctuation amplitude of GWT is the largest in the ETP and the smallest in the TIP. The fluctuation amplitude of GWT in the seasonal frost zone and discontinuous permafrost zone is still more significant during the EFP, while the fluctuation amplitude of GWT in the continuous permafrost zone is significantly reduced during the EFP. The recharge and discharge capacity of groundwater has the strongest impact on the groundwater during the ETP. The effect of discharge on groundwater in seasonal frost zones and discontinuous permafrost zones is still significant during the EFP, while the impact in continuous permafrost regions is significantly reduced.

This study only conducted some exploratory analysis in the middle of QTP. In the later stage, it is necessary to further grasp the long sequence monitoring data of GWT, supplement the monitoring data of ALT near the monitoring well, carry out a deeper analysis from the mechanism, and analyze the characteristics of GWT change.

Acknowledgments

The study was supported by the National Natural Science Foundation of China (No. 52022110 and No. 51879276), and the Second Tibetan Plateau Scientific Expedition and Research Program (No. 2019QZKK0207). In addition, the authors thank the anonymous researchers and editors who served with some valuable data and suggestions to enhance the manuscript.

Conflict of Interest

The authors declare no conflict of interest.

References

1. IMMERZEEL W.W., VAN B.L.P., BIERKENS M.F. Climate change will affect the Asian Water Towers. *Science*, **328** (5984), 1382, **2010**.
2. YANG Y.H., WENG B.S., YAN D.H., GONG X.Y., DAI Y.Y., NIU Y.Z., DONG G.Q. Tracing potential water sources of the Nagqu river using stable isotopes. *Journal of Hydrology: Regional Studies*, **34**, 100807, **2021**.
3. YANG K., WU H., QIN J., LIN C.G., TANG W.J., CHEN Y.Y. Recent climate changes over the Tibetan Plateau and their impacts on energy and water cycle: A review. *Global and Planetary Change*, **112**, 79, **2014**.
4. ZHONG Q.Z., QING B.W., GUAN L.J., SIRU G., JI C., YONG Z.L. Changes in the permafrost temperatures from 2003 to 2015 in the Qinghai-Tibet Plateau. *Cold Regions Science and Technology*, **169**, 102904, **2020**.
5. CHENG G.D., WU T.H. Responses of permafrost to climate change and their environmental significance, Qinghai-Tibet Plateau. *Journal of Geophysical Research*, **112** (F2), **2007**.
6. JIN H.J., HE R.X., CHENG G.D., WU Q.B., WANG S.L., LU L.Z., CHANG X.L. Changes in frozen ground in the source area of the Yellow River on the Qinghai-Tibet Plateau, China, and their eco-environmental impacts. *Environmental Research Letters*, **4** (4), **2009**.
7. ZHAO D.S., WU S.H. Projected changes in permafrost active layer thickness over the Qinghai-Tibet Plateau under climate change. *Water Resources Research*, **55** (9), 7860, **2019**.
8. ZOU D.F., ZHAO L., SHENG Y., CHEN J., HU G.J., WU T.H., WU J.C. A new map of permafrost distribution on the Tibetan Plateau. *The Cryosphere*, **11** (6), 2527, **2017**.
9. ZOU F., TENZER R., JIN S. Water storage variations in Tibetan Plateau from grace, icesat, and hydrological data. *Remote Sensing*, **11** (9), **2019**.
10. GUO X.Y., FENG Q., YIN Z.L., SI J., XI H.Y., ZHAO Y. Critical role of groundwater discharge in sustaining streamflow in a glaciated alpine watershed, northeastern Tibetan Plateau. *Sci Total Environ*, **822**, 153578, **2022**.
11. HAYASHI M. Alpine hydrogeology: The critical role of groundwater in sourcing the headwaters of the world. *Ground Water*, **58** (4), 498, **2020**.
12. DAI L., GUO X., DU Y., ZHANG F., KE X., CAO Y., LI Y., LI Q., LIN L., CAO G. The response of shallow groundwater levels to soil freeze-thaw process on the Qinghai-Tibet Plateau. *Ground Water*, **57** (4), 602, **2019**.
13. MA R., SUN Z.Y., CHANG Q.X., GE M.Y., PAN Z. Control of the interactions between stream and groundwater by permafrost and seasonal frost in an alpine catchment, northeastern Tibet-Plateau, China. *Journal of Geophysical Research: Atmospheres*, **126** (5), **2021**.
14. GREEN T.R., TANIGUCHI M., KOOI H., GURDAK J.J., ALLEN D.M., HISCOCK K.M., TREIDEL H., AURELI A. Beneath the surface of global change: Impacts of climate change on groundwater. *Journal of Hydrology*, **405** (3-4), 532, **2011**.
15. MA R., SUN Z.Y., HU Y.L., CHANG Q.X., WANG S., XING W.L., GE M.Y. Hydrological connectivity from glaciers to rivers in the Qinghai-Tibet Plateau: Roles of suprapermfrost and subpermafrost groundwater. *Hydrology and Earth System Sciences*, **21** (9), 4803, **2017**.
16. CHEN J.L., FAMIGLIETT J.S., SCANLON B.R., RODELL M. Groundwater storage changes: Present status from grace observations. In *Remote Sensing and Water Resources*: Springer, 207, **2016**.
17. QI W., LIU J.G., YANG H., CHEN D.L., FENG L. Assessments and corrections of Gldas2.0 forcing data in four large transboundary rivers in the Tibetan Plateau and Northeast China. *Earth and Space Science*, **9** (1), **2021**.
18. WANG S.B., XIE Z., WANG F.L., ZHANG Y.Q., WANG W.P., LIU K., QI Z.X., ZHAO F.Y., ZHANG G.Q., XIAO Y. Geochemical characteristics and quality appraisal of groundwater from huatugou of the Qaidam basin on the Tibetan Plateau. *Frontiers in Earth Science*, **10**, **2022**.
19. CHENG G.D., JIN H.J. Permafrost and groundwater on the Qinghai-Tibet Plateau and in northeast China. *Hydrogeology Journal*, **21** (1), 5, **2012**.
20. JIN H.J., HUANG Y.D., BENISE, V.F., MA Q., MARCHENKO S.S., SHEPELEV V.V., HU Y., LIANG S.H. Permafrost degradation and its hydrogeological impacts. *Water*, **14** (3), **2022**.
21. CHANG J., WANG G.X., LI C.J., MAO T.X. Seasonal dynamics of suprapermfrost groundwater and its response to the freezing-thawing processes of soil in the permafrost region of Qinghai-Tibet Plateau. *Science China Earth Sciences*, **58** (5), 727, **2015**.
22. HUANG K.W., DAI J.C., WANG G.X., CHANG J., LU Y.Q., SONG C.L., HU Z.Y., AHMED N., YE R.Z. The impact of land surface temperatures on suprapermfrost groundwater on the central Qinghai-Tibet Plateau. *Hydrological Processes*, **34** (6), 1475, **2019**.
23. WANG J.Y., LUO S.Q., LV Z.B., LI W.J., TAN X.Q., DONG Q.X., CHEN Z.H. Improving ground heat flux estimation: Considering the effect of freeze/thaw process on the seasonally frozen ground. *Journal of Geophysical Research: Atmospheres*, **126** (24), **2021**.
24. GAO M., CHEN X., WANG J., SOULSBY C., CHENG Q. Climate and landscape control on Spatio-temporal patterns of stream water stable isotopes in a large glacierized mountain basin on the Tibetan Plateau. *Sci Total Environ*, **771**, 144799, **2021**.
25. MAGHREBI M., NOORI R., PARTANI S., ARAGHI A., BARATI R., FARNOUSH H., TORABI H.A. Iran's groundwater hydrochemistry. *Earth and Space Science*, **8** (8), **2021**.
26. MENG Y., LIU G. Isotopic characteristics of precipitation, groundwater, and stream water in an alpine region in southwest China. *Environmental Earth Sciences*, **75** (10), **2016**.
27. MENG Y., LIU G., LI M. Tracing the sources and processes of groundwater in an alpine glacierized region in southwest China: Evidence from environmental isotopes. *Water*, **7** (12), 2673, **2015**.
28. YANG Y.Z., WU Q.B., JIN H.J., WANG Q.F., HUANG Y.D., LUO D.L., GAO S.H., JIN X.Y. Delineating the hydrological processes and hydraulic connectivities under permafrost degradation on northeastern Qinghai-Tibet Plateau, China. *Journal of Hydrology*, **569**, 359, **2019**.
29. ABIYE T., MASINDI K., MENGISTU H., DEMLIE M. Understanding the groundwater-level fluctuations for better management of groundwater resource: A case in the Johannesburg region. *Groundwater for Sustainable Development*, **7**, 1, **2018**.
30. BUI DD., KAWAMURA A., TONG T.N. Spatio-temporal analysis of recent groundwater-level trends in the Red River Delta, Vietnam. *Hydrogeology Journal*, **20** (8), 1635, **2012**.
31. YANG Y.H., WENG B.S., MAN Z.H., YU Z.L., ZHAO J.L. Analyzing the contributions of climate change and

- human activities on runoff in the northeast Tibet Plateau. *Journal of Hydrology: Regional Studies*, **27**, 100639, **2020**.
32. DONG G.Q., WENG B.S., CHEN J., YAN D.H., WANG H. Variation characteristics of stable isotopes in water along main stream of Naqu river in source area of Nujiang river. *China Institute of Water Resources and Hydropower Research*, **49** (08),108, **2018**.
 33. DENG C., ZHANG W. Spatiotemporal distribution and the characteristics of the air temperature of a river source region of the Qinghai-Tibet Plateau. *Environ Monit Assess*, **190** (6), 368, **2018**.
 34. MARMY A., SALZMANN N., SCHERLER M., HAUCK C. Permafrost model sensitivity to seasonal climatic changes and extreme events in mountainous regions. *Environmental Research Letters*, **8** (3), **2013**.
 35. ZHU X.F., WU T.H., NI J., WU X.D., HU G.J., WANG S.J., LI X.F., WEN A., LI R., SHANG C.P., MA X. Increased extreme warming events and the differences in the observed hydrothermal responses of the active layer to these events in China's permafrost regions. *Climate Dynamics*, **2022**.
 36. EVANS S.G., GE S., LIANG S.H. Analysis of groundwater flow in mountainous, headwater catchments with permafrost. *Water Resources Research*, **51** (12), 9564, **2015**.
 37. WALVOORD M.A., VOSS C.I., WELLMAN T.P. Influence of permafrost distribution on groundwater flow in the context of climate-driven permafrost thaw: Example from Yukon flats basin, Alaska, United States. *Water Resources Research*, **48** (7), **2012**.
 38. WAN C.W., LI K., SHEN S.C., GIBSON J.J., JI K.F., YI P., YU Z.B. Using tritium and ²²²Rn to estimate groundwater discharge and thawing permafrost contributing to surface water in permafrost regions on Qinghai-Tibet Plateau. *Journal of Radioanalytical and Nuclear Chemistry*, **322** (2), 561, **2019**.
 39. ZHOU W., WENG B.S., YAN D.H. Evaluation for short-duration freeze-thaw events of seasonally frozen soil in the headstreams of Nujiang river. *South-to-North Water Transfers and Water Science & Technology*, **1**, **2022**.
 40. MAN Z.H., WENG B.S., YANG Y.H., GONG X.Y., LI M., YU, Z.L. Effects of the freezing-thawing cycle mode on alpine vegetation in the Nagqu River Basin of the Qinghai-Tibet Plateau. *Water*, **11** (10), 2122, **2019**.
 41. LYU H., WU T.T., SU X.S., WANG Y.Q., WANG C., YUAN Z.J. Factors controlling the rise and fall of groundwater level during the freezing-thawing period in seasonal frozen regions. *Journal of Hydrology*, **606**, 127442, **2022**.
 42. XIE H.Y., JIANG X.W., TAN S.C., WAN L., WANG X.S., LIANG S.H., ZENG Y.J. Interaction of soil water and groundwater during the freezing-thawing cycle: Field observations and numerical modeling. *Hydrology and Earth System Sciences*, **25** (8), 4243, **2021**.
 43. CHANG Q.X., MA R., SUN Z.Y., ZHOU A.G., HU Y.L., LIU Y.G. Using isotopic and geochemical tracers to determine the contribution of glacier-snow meltwater to streamflow in a partly glacierized alpine-gorge catchment in northeastern Qinghai-Tibet Plateau. *Journal of Geophysical Research: Atmospheres*, **123** (18), 10,037, **2018**.
 44. COCHAND M., MOLSON J., LEMIEUX J.M. Groundwater hydrogeochemistry in permafrost regions. *Permafrost and Periglacial Processes*, **30** (2), 90, **2019**.
 45. GONG X.Y., WENG B.S., YAN D.H., YANG Y.H., NIU Y.Z., WANG H. Potential recharge sources and origin of solutes in groundwater in the central Qinghai-Tibet Plateau using hydrochemistry and isotopic data. *Journal of Hydrology: Regional Studies*, **40**, 101001, **2022**.
 46. HU Y.L., MA R., WANG Y.X., CHANG Q.X., WANG S., GE M.Y., BU J.W., SUN Z.Y. Using hydrogeochemical data to trace groundwater flow paths in a cold alpine catchment. *Hydrological Processes*, **33** (14), 1942, **2019**.
 47. CHANG J., YE R.Z., WANG G.X. Review: Review: Progress in permafrost hydrogeology in China. *Hydrogeology Journal*, **26** (5), 1387, **2018**.
 48. CHENG G.D., JIN H.J. Groundwater in the permafrost regions on the Qinghai-Tibet Plateau and it changes. *Hydrogeology & Engineering Geology*, **40** (01), 1, **2013**.
 49. WU J.C., SHENG Y., WU, Q.B., LI J., ZHANG X.M. Discussion on the possibility of taking ground ice in permafrost regions as water sources under climate warming. *Journal of Glaciology and Geocryology*, **31**(02), 350, **2009**.
 50. HAO S., LI F.D., LI Y.H., GU, C.K., ZHANG Q.Y., QIAO Y.F., JIAO L., ZHU N. Stable isotope evidence for identifying the recharge mechanisms of precipitation, surface water, and groundwater in the Ebinur Lake Basin. *Science of the Total Environment*, **657**, 1041, **2019**.
 51. BARNHART T.B., MOLOTCH N.P., LIVNEH B., HARPOLD A.A., KNOWLES J.F., SCHNEIDER D. Snowmelt rate dictates streamflow. *Geophysical Research Letters*, **43** (15), 8006, **2016**.
 52. EVANS S.G., GE S., VOSS C.I., MOLOTCH N.P. The role of frozen soil in groundwater discharge predictions for warming alpine watersheds. *Water Resources Research*, **54** (3), 1599, **2018**.
 53. WENG B.S., YANG Y.H., YAN D.H., WANG J.W., DONG G.Q., WANG K., QIN T.L., DORJSUREN B. Shift in plankton diversity and structure: Influence of runoff composition in the Nagqu river on the Qinghai-Tibet Plateau. *Ecological Indicators*, **109**, 105818, **2020**.
 54. BENSE V.F., FERGUSON G., KOOI H. Evolution of shallow groundwater flow systems in areas of degrading permafrost. *Geophysical Research Letters*, **36** (22), **2009**.
 55. GURTZ J., ZAPPA M., JASPER K., LANG H., VERBUNT M., BADOUX A., VITVAR T. A comparative study in modeling runoff and its components in two mountainous catchments. *Hydrological Processes*, **17** (2), 297, **2003**.
 56. SMITH L.C., PAVELSKY T.M., MACDONALD G.M., SHIKLOMANOV A.I., LAMMERS R.B. Rising minimum daily flows in northern Eurasian rivers: A growing influence of groundwater in the high-latitude hydrologic cycle. *Journal of Geophysical Research: Biogeosciences*, **112** (G4), **2007**.
 57. GUO L.D., CAI Y.H., BELZILE C., MACDONALD R.W. Sources and export fluxes of inorganic and organic carbon and nutrient species from the seasonally ice-covered Yukon river. *Biogeochemistry*, **107** (1-3), 187, **2010**.